ELSEVIER

Engineering Structures 24 (2002) 923–932

ENGINEERING STRUCTURES

www.elsevier.com/locate/engstruct

Concrete confined by FRP material: a plasticity approach

A.I. Karabinis *, T.C. Rousakis

Laboratory of Reinforced Concrete, Department of Civil Engineering, Democritus University of Thrace, Vas. Sophia's 1, Xanthi 671 00, Greece

Received 20 June 2001; received in revised form 3 January 2002; accepted 3 January 2002

Abstract

Carbon fiber-reinforced polymer (FRP) material has proved to be more efficient than other composites when applied to concrete columns as an external reinforcement. Because of its enhanced durability characteristics compared to glass or aramid, and its relatively high *E*-modulus, carbon FRP shows a higher confining performance. The behavior of 22 cylindrical 200×320 mm specimens (height to diameter ratio 1.6) that are externally wrapped by carbon FRP sheets in low volumetric ratios (0.23–0.7%) is presented. The specimens are subjected to axial monotonic load until failure occurs. Carbon FRP confinement, even in low volumetric ratios, seems to considerably increase the strength and especially the ductility of concrete. A constitutive model based on plasticity theory is applied. The model proposed and applied to steel-confined concrete in this paper is modified and calibrated so as to incorporate the dilation characteristics of the FRP-confined concrete. The model provides the stress–strain curves of axially loaded circular columns that are confined by FRP reinforcement. It can be used in FRP tube-encased concrete as well as in FRP sheet-wrapped concrete. Satisfactory correlation of experimental and analytical results is observed.

Keywords: Carbon FRP; Confinement; Stress–strain curves; Plasticity theory; Axial loading; External reinforcement; Wrapping

1. Introduction

During the past decade efforts have been increasingly concentrated on the replacement of the conventional steel reinforcement in concrete elements by fiber-reinforced polymer (FRP) reinforcement. Concerning its confining characteristics, FRP reinforcement has a linear elastic behavior up to failure and exerts an ever-increasing confining pressure on the concrete core. The result of the developed confining mechanism is a considerable enhancement in the strength and ductility of concrete when loaded axially [1–4]. FRP reinforcement has many advantages, as it is easy to transfer (low weight to volumetric ratio) and to apply in the construction field, and exhibits high corrosion resistance in harsh conditions [5,6]. In particular, carbon FRP, of all the composites, shows high durability and an *E*-modulus comparable to steel or even higher.

The modeling of the behavior of FRP-confined concrete is mostly based on semiempirical equations [3,7] while there are models based on constitutive relationships [8,9]. The stress–strain response provided is strongly dependent on the resulting experimental data. This disadvantage can be overcome by using the theory of plasticity as it has been successfully applied in steel-confined concrete [10].

In this paper the results of the behavior of 22 cylindrical specimens confined by carbon FRP sheets under axial load are presented. The specimens are wrapped with relatively low confinement volumetric ratios (ρ_j) 0.23–0.7% so as to examine their confining effect when FRP sheets are used as reinforcement in rehabilitation. In addition, a constitutive model based on the plasticity theory is applied. The model that is proposed and applied to steel-confined concrete in this paper is modified and calibrated so as to incorporate the dilation characteristics of the FRP-confined concrete. The model provides the stress–strain curves of axially loaded circular columns that are confined by FRP reinforcement. It can be used in FRP tube-encased concrete as well as in FRP sheet-wrapped concrete. Satisfactory correlation of experimental and analytical results is observed.

* Corresponding author. Fax: +30-541-26932.
E-mail address: karabin@civil.duth.gr (A.I. Karabinis).

0141-0296/02/$ - see front matter
PII: S0141-0296(02)00011-1

Table 1
Mixtures[a] and experimental program

	Type A (C20/25)	Type B (C16/20)
Aggregate diameter 13–31.5 mm	0.715	0.700
Aggregate diameter 5–13 mm	0.120	0.120
Aggregate diameter 0–5 mm	0.220	0.350
Aggregate diameter 0–5 mm	0.690	0.650
Cement I-45	0.030	–
Cement I-35	0.320	0.310
Water	0.180	0.180
Additives	0.050	0.050
z (cement)/*k* (gravel)/*w* (water)	0.350/1.745/0.18	0.310/1.82/0.18
Slump *s* (cm)	7	3.5
Water to cement ratio (*w*/*z*)	0.51	0.58
Total of confined specimens	9	9

[a] Mix proportions by weight.

Table 2
Mechanical properties of carbon sheet (per layer) C 240 (S&P Sintecno [11])

Weight (g/m^2)	Design carbon fiber thickness (mm)	Elasticity modulus of carbon fibers (GPa)	Elongation at failure (‰)
200	0.117	240	15.5

2. Experimental program

For the construction of the specimens two concrete mixtures were used, type A and type B with strength 47.5 and 43.5 MPa, respectively. The modulus of elasticity for the two types of concrete was 24.5 and 23.5 GPa, respectively. The proportion of the mixtures is presented in Table 1.

Twenty-two cylindrical specimens with dimensions 200×320 mm (height to diameter ratio 1.6) were tested. Eighteen of the specimens were confined by S&P C240 carbon FRP [11] unidirectional sheet with width 300 mm. Table 2 shows the mechanical properties of the carbon sheet. In every triad of identical specimens, one, two and three layers of carbon sheet were applied (Table 3).

Table 3
Thickness of carbon sheet per specimen

	Type A (C20/25)	Type B (C16/20)
Carbon sheet thickness/layer (mm)	0.117	0.117
Labels		
Unconfined	A1, A2	B1, B2
1 layer	C1, C2, C3	C4, C5, C6
2 layers	C7, C8, C9	C10, C11, C12
3 layers	C13, C14, C15	C16, C17, C18

The carbon sheet was glued by using a two-component epoxy resin.

All specimens were wrapped with orientation perpendicular to their axis having an overlap of 160 mm (a quarter of specimen perimeter) in the external layer. Wrapped cylinders remained in laboratory conditions for more than 12 days after gluing. The concrete specimens were tested 56 days after casting, subjected to axial monotonic load under a displacement control mode with a constant rate of 3×10^{-5} mm/mm/s. For the measurement of average axial strains a linear voltage displacement transformer (LVDT) was used.

2.1. Experimental results

Typical failure of wrapped specimens was very noisy followed by an "explosive" fracture of the carbon fiber sheet. Failure started at the middle height of the specimens with a sudden or gradual development in strips of carbon FRP sheet (Fig. 1a). Premature failure occurred in some specimens (C3 and C14) due to local failure of the carbon FRP sheet (Fig. 1b). In some specimens (C8 and C10) a failure at the overlap was observed (Fig. 1c).

The stress–strain response of the specimens of types A and B with 0.23% confinement volumetric ratio (1 layer) is presented in Fig. 2. The response is bilinear, with the second branch somewhat horizontal revealing a ductile behavior with a slight increase in strength. Cylinders with two and three layers of carbon FRP sheet (Figs. 3 and 4) show a similar bilinear behavior. The limit between the two distinct regions is around the stress–strain values of unconfined concrete at maximum strength. By increasing the stiffness of the confining reinforcement, the second branch of the stress–strain response ascends, resulting in a higher strength and higher strain at failure (Table 4, Figs. 5 and 6).

The energy absorption capacity of the composite system indicates the effectiveness of the FRP confinement. The energy absorption is measured for all the specimens (Table 4 and Fig. 7) using the expression:

$$E = \sum(\mathrm{d}\sigma\,\mathrm{d}\varepsilon).$$

The increase in strength, axial strain at failure and energy absorption for higher confinement volumetric ratio indicates significant enhancement of the mechanical behavior of the concrete.

The variation of results denotes the need for the determination of minimum values of volumetric ratio of reinforcement along with development of FRP application guidelines and quality control for the elimination of such problems.

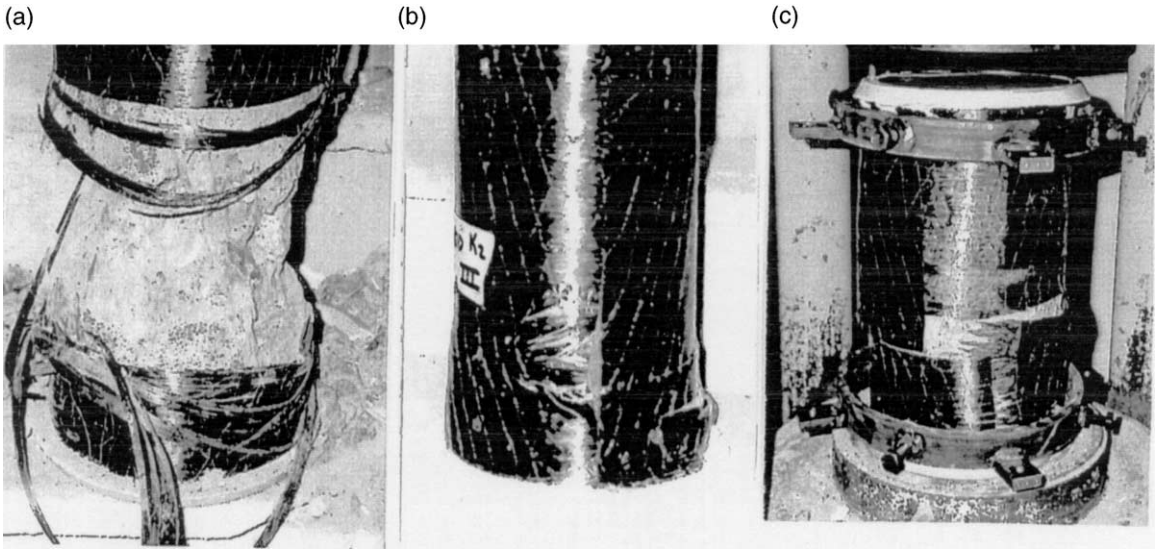

Fig. 1. Specimens after failure.

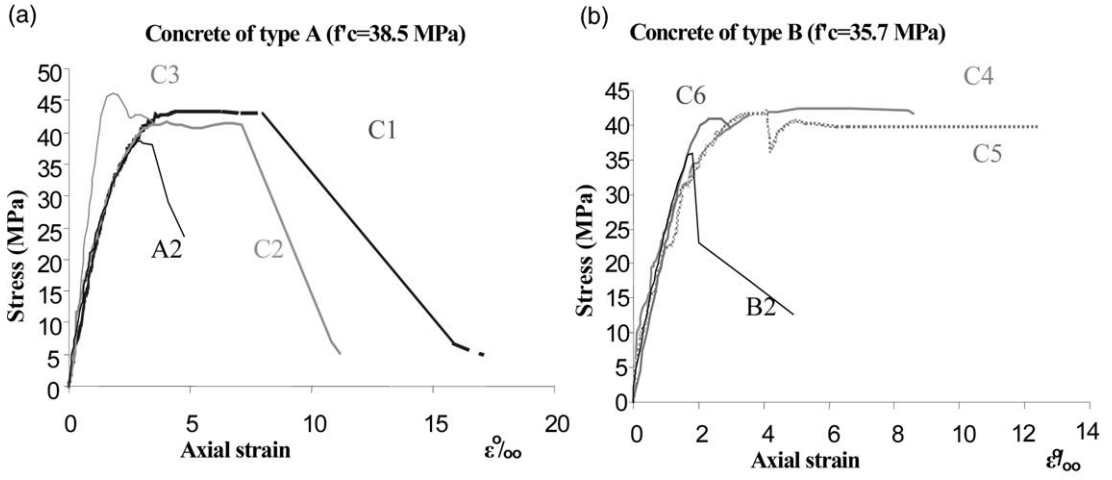

Fig. 2. Stress–strain diagram for concrete types A and B confined with one layer of carbon FRP sheet.

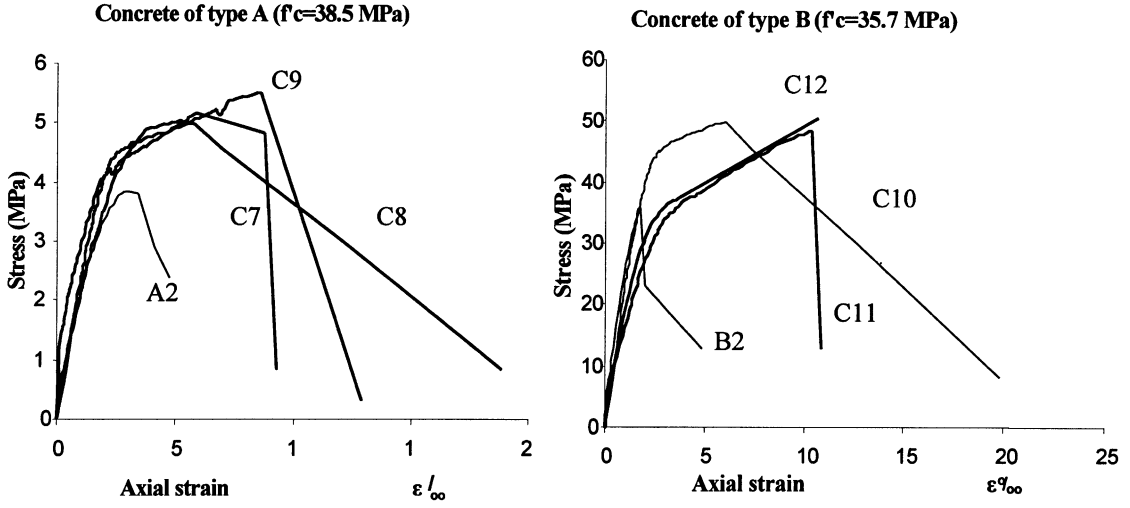

Fig. 3. Stress–strain diagram for concrete types A and B confined with two layers of carbon FRP sheet.

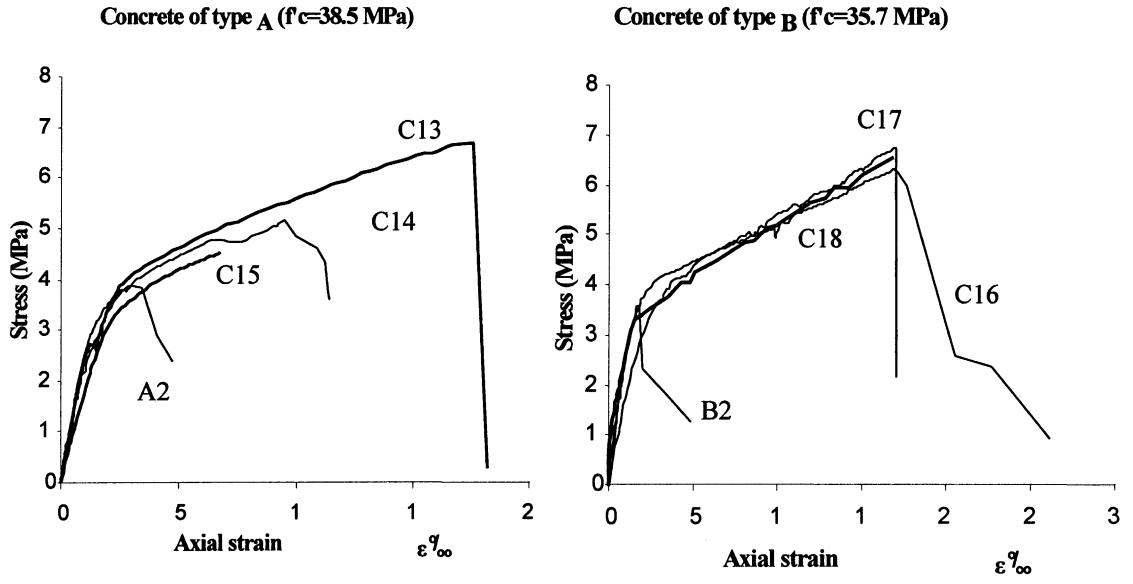

Fig. 4. Stress–strain diagram for concrete types A and B confined with three layers of carbon FRP sheet.

Table 4
Experimental results

Specimen		Ultimate strength $f'_{c\,max}$ (MPa)	Ultimate axial strain ε_{cu} (‰)	Ultimate load/load of unconfined $P_{c\,max}/P_{co}$	Ultimate strain/strain of unconfined $\varepsilon_{cu}/\varepsilon_{co}$	Absorbed energy (MJ/m^3)
Type A (C20/25)						
A1		40.9	2.72	–	–	0.097
Á2		38.5	2.80	1.00	1.00	0.094
1 layer	C1	43.0	7.96	1.12	2.84	0.288
	C2	41.6	7.14	1.08	2.55	0.236
	C3	46.0	3.49	1.19	1.25	0.123
2 layers	C7	51.5	8.77	1.34	3.13	0.377
	C8	50.0	5.77	1.30	2.06	0.222
	C9	55.0	8.60	1.43	3.07	0.367
3 layers	C13	67.0	17.60	1.74	6.29	0.897
	C14	51.5	10.90	1.34	3.89	0.447
	C15	45.0	6.72	1.17	2.40	0.221
Type B (C16/20)						
	B1	33.9	2.02	–	–	0.051
	B2	35.7	1.80	1.00	1.00	0.046
1 layer	C4	42.5	8.59	1.19	4.77	0.322
	C5	42.0	12.38	1.18	6.88	0.457
	C6	41.0	2.96	1.15	1.64	0.083
2 layers	C10	50.0	6.04	1.40	3.36	0.233
	C11	48.5	10.4	1.36	5.78	0.374
	C12	50.0	10.72	1.40	5.96	0.403
3 layers	C16	63.0	17.18	1.76	9.54	0.824
	C17	67.5	17.05	1.89	9.47	0.817
	C18	65.5	16.86	1.83	9.37	0.801

3. Confinement modeling

The theory of plasticity has been used to reproduce the behavior of steel-confined concrete as, unlike semi-empirical models, it provides a sound theoretical basis. A non-associative flow rule for the concrete is adopted. Plasticity models have been developed mostly for use in finite element codes. However, it has been demonstrated [10,12,13] that the behavior of simple structural members can be accurately estimated using a Drucker–Prager-type constitutive model. In this study the above model is properly modified and calibrated so as to provide the FRP-confined concrete stress–strain response.

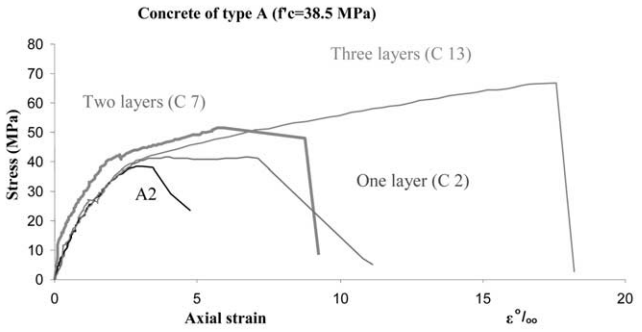

Fig. 5. Effect of thickness of carbon FRP sheet on stress–strain behavior for confined concrete type A.

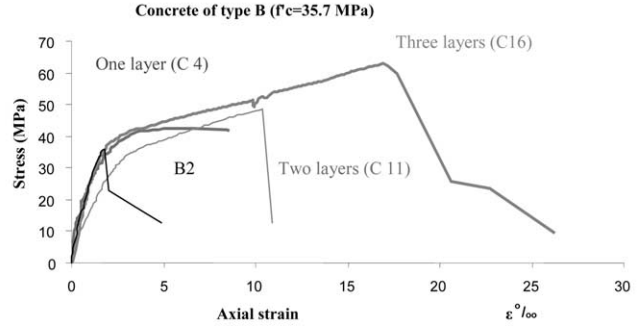

Fig. 6. Effect of thickness of carbon FRP sheet on stress–strain behavior for confined concrete type B.

3.1. Brief model presentation

In this confinement model [10,12,13,17] concrete responds as an elasto-plastic material following a Drucker–Prager-type [14] hardening–softening criterion. The plasticity functions that are used for this purpose are the loading function F, the hardening function κ, and the potential function G. The mathematical expression for the loading function F is:

$$F = \sqrt{J_{2D}} + \theta J_1 - \kappa = 0, \tag{1}$$

where $J_{2D} = 1/6([\sigma_1-\sigma_2]^2 + [\sigma_2-\sigma_3]^2 + [\sigma_3-\sigma_1]^2)$ is the second invariant of the deviatoric stress, $J_1=\sigma_1+\sigma_2+\sigma_3$ is the first invariant of the stress, θ is a frictional parameter to express the pressure sensitivity of the material and κ is a strain hardening–softening function. For the hardening–softening κ the plastic strain trajectory $\hat{\varepsilon}$ is used:

$$\hat{\varepsilon} = \int \sqrt{\mathrm{d}\varepsilon^{\mathrm{p}^{\mathrm{T}}}\,\mathrm{d}\varepsilon^{\mathrm{p}}}, \tag{2}$$

where superscript p indicates irrecoverable deformations and the superscript T denotes transpose operation. The mathematical expression for κ is:

$$\kappa = \bar{\theta}\left(\frac{\bar{\varepsilon}}{\dfrac{1}{K_1} + \dfrac{\bar{\varepsilon}}{f'\mathrm{u}-f'\mathrm{y}}} - R(\sigma_3)K_2\bar{\varepsilon} + f'\mathrm{y}\right), \tag{3}$$

where $\bar{\theta}$ is a constant that allows the uniaxial interpretation of the loading function F:

$$\bar{\theta} = \frac{1}{\sqrt{3}} - \theta, \tag{4}$$

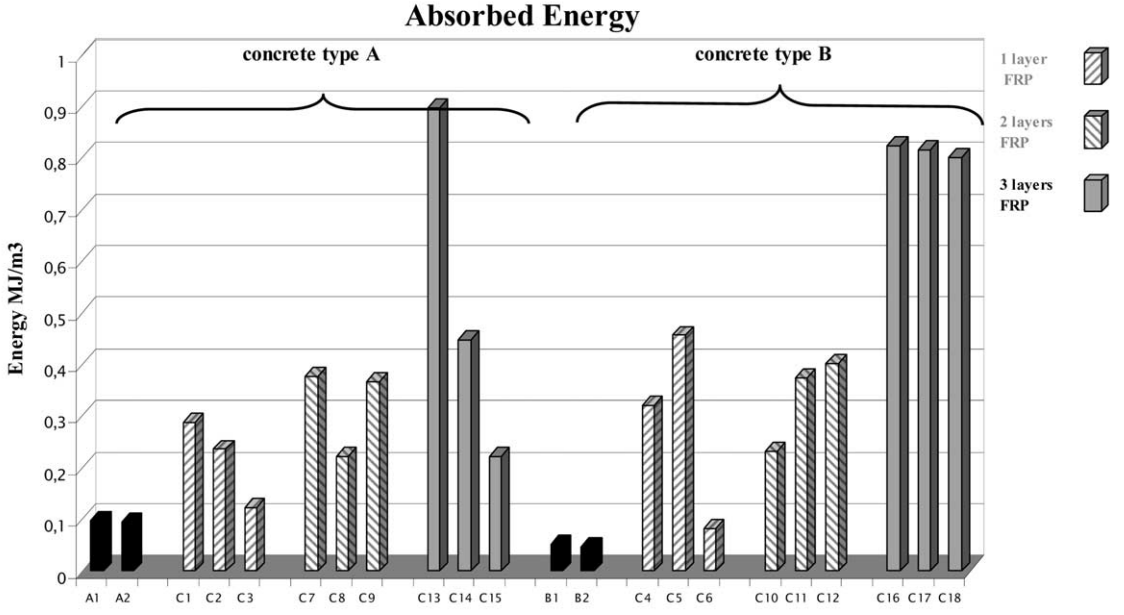

Fig. 7. Energy absorption of all specimens.

$\bar{\varepsilon}$ is a function of $\hat{\varepsilon}$:

$$\bar{\varepsilon} = \frac{2\hat{\varepsilon}}{\alpha - 1}, \tag{5}$$

and α is the dilatation of concrete under unconfined compression. The dilatation α is the slope of the $I_1^p - \sqrt{I_{2D}^p}$ diagram, where I_1^p and I_{2D}^p are the invariants of plastic strain. It can be shown that for a triaxial test:

$$d\varepsilon_3^p = \frac{1 + \frac{\alpha}{\sqrt{3}}}{\frac{\alpha}{\sqrt{3}} - 2} d\varepsilon_1^p, \tag{6}$$

thus the dilatation α is modeled by the asymptotic relation:

$$\alpha = \alpha_o - \frac{\hat{\varepsilon}}{\frac{1}{K_\alpha} - \frac{\hat{\varepsilon}}{\alpha_u - \alpha_o}}, \tag{7}$$

where α_o and α_u are the initial and ultimate values of α and K_α is the initial rate of change of α as a function of $\hat{\varepsilon}$. K_1 is the initial plastic modulus, K_2 is the post-peak slope of the unconfined compression stress–strain curve and f'_y is the elastic limit in uniaxial compression (equal to $f'_c/4$). The ultimate strength of concrete f'_u is expressed as:

$$f'u = f'y + (f'c - f'y)\frac{K_1}{(\sqrt{K_1} - \sqrt{K_2})^2}. \tag{8}$$

Finally, $R(\sigma_3)$ is the damage function modeled by the equation:

$$R(\sigma_3) = e^{\chi\sigma_3}, \tag{9}$$

where the damage rate is controlled by the amount of confinement σ_3 and the material parameter χ. The plastic strain rates are given by the flow rule:

$$d\varepsilon^p = d\lambda \frac{dG}{d\sigma}, \tag{10}$$

where G is the potential function:

$$G = \sqrt{I_{2D}} + \beta J_1, \tag{11}$$

and $\beta = \alpha/6$.

The incremental elasto-plastic constitutive relation is based on the plasticity theory:

$$d\sigma = D\, d\varepsilon, \tag{12}$$

where the elasto-plastic constitutive matrix D is given by:

$$D = E - \frac{E\frac{\partial G}{\partial \sigma}\frac{\partial F^T}{\partial \sigma}E}{\frac{\partial F^T}{\partial \sigma}E\frac{\partial G}{\partial \sigma} + \frac{\partial F}{\partial \hat{\varepsilon}}\sqrt{\frac{\partial G^T}{\partial \sigma}\frac{\partial G}{\partial \sigma}}}. \tag{13}$$

Integration of Eq. (12) provides the stress–strain relation for concrete under any arbitrary loading.

The behavior of composite sheet is linear elastic up to its failure. For all practical applications of FRP confinement, uniaxial modeling is used. The mechanical behavior of typical FRP sheet in comparison to steel is presented in Fig. 8.

The development of uniform lateral stresses can be assumed in the case of cylindrical concrete element sheet, fiber or tube confinement. The stresses that are directly related to the stiffness of the confining mean and the respective lateral expansion of the concrete are calculated with an iterative procedure. The basic assumption of the model is the strain compatibility between concrete expansion and the confining mean.

3.2. Failure criterion

For FRP-confined concrete the compressive axial strain of concrete at failure is obtained when $\varepsilon_l = \varepsilon_{ju}$, that is when the lateral strain of concrete reaches the strain at failure of the FRP confining reinforcement.

3.3. Calibration of material parameters

For the analytical model description, 14 material parameters are used to reproduce concrete behaviour:

- Two elastic parameters: modulus of elasticity E and Poisson's ratio ν
- Three failure–yield parameters: f'_y, f'_c and θ
- Six hardening parameters: K_1, K_2, χ_1, χ_2, $\hat{\varepsilon}_1$ and $\hat{\varepsilon}_2$
- Three dilatation parameters: α_0, α_u and K_α

The frictional parameter θ is replaced by the more common "angle of internal friction" φ where:

$$\theta = \frac{2\sin\phi}{\sqrt{3}(3 - \sin\phi)}. \tag{16}$$

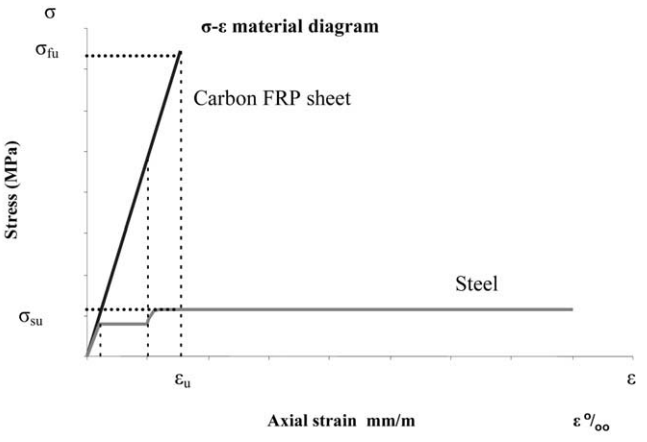

Fig. 8. Mechanical behavior for typical structural steel reinforcement and carbon composite material.

Table 5
Input of used experimental data

Experiment	f'_c (MPa)	t_j (m)	f_{ju} (MPa)	E_j (MPa)	E_{pj} (MPa)	ε_{op}
6 layers E-glass FRP[a] [2]	32	0.0013	524	37233	37233	1
10 layers E-glass FRP[a] [2]	32	0.0021	579	40336	40336	1
14 layers E-glass FRP[a] [2]	32	0.003	641	40749	40749	1
4 layers E-glass FRP [15]	36.3	0.0012	583	52000	52000	1
5 layers S-glass FRP Mastrapa (1997)	37.2	0.0031	586	20600	20600	1
1 layer carbon FRP[b] [16]	38.5	0.000117	3720	240000	240000	1
2 layers carbon FRP[c] [16]	35.7	0.000234	3720	240000	240000	1
3 layers carbon FRP[d] [16]	38.5	0.000351	3720	240000	240000	1

[a] Batch C
[b] specimen C2
[c] specimen C11
[d] specimen C13

The inelastic parameters of the model are calibrated using several experimental results referred to cylindrical FRP-confined specimens (Table 5). The experiments included confining materials with low and high E-modulus, as well as a wide range of confinement volumetric ratios (0.234–8.11%). The final material parameters are presented in Table 6, where it is indicated that they can be reasonably associated to the unconfined strength of concrete f'_c. It should be noted that the extension of strengths of concrete to a wider range is necessary.

4. Evaluation of model

A number of experimental results that refer to FRP-confined concrete have been used to evaluate the accuracy of the model. They cover a variety of confining techniques using FRP jackets (sheets), FRP tubes and fibers wrapped on the surface of concrete. The proposed model is also compared against three existing models by Samaan et al. [3], Saafi et al. [7] and Spoelstra and Monti [9]. The values are cut for all models to the ultimate experimental strain value.

4.1. Concrete cylinders encased in glass FRP tubes

Concrete cylinders encased in FRP tubes were tested by Mirmiran and Shahawy [2]. Twenty-four concrete-filled FRP tubes and six plain concrete specimens (152.5×305 mm) were tested. The mechanical properties of the specimens were f'_{co}=32 MPa, ε_{co}=0.002 and E_c=30 000 MPa. The reported hoop strengths for the FRP tubes were 37 233 MPa for the six-layer E-glass FRP tube, 40 336 MPa for the 10-layer E-glass FRP tube and 40 749 MPa for the 14-layer E-glass FRP tube. In Figs. 9–11 the predicted stress–strain curves of the four models are showed against experimental results.

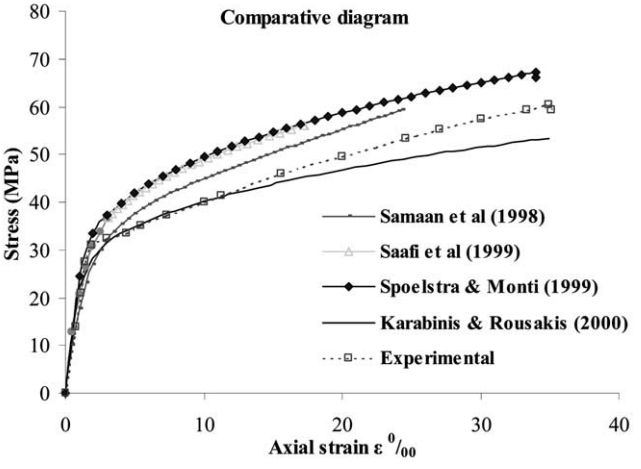

Fig. 9. Comparison of experimental σ–ε values with analytical prediction for specimen of batch C from Mirmiran and Shahawy [2] (six layers of E-glass FRP tube).

Table 6
Material parameters for concrete, related to f'_c

f'_c (Mpa)	E (MPa)	f'_y (MPa)	φ (deg)	α_o	α_u	K_α	K_1 (GPa)	K_2 (MPa)	χ_1 (MPa^{-1})	χ_2 (MPa^{-1})	$\hat{\varepsilon}_1$	$\hat{\varepsilon}_2$
32	32240	8	48	−0.6	$-\sqrt{3}$	60	110	7	0.3	0.8	0.007	0.06
36.3	34344	9	48	−0.6	$-\sqrt{3}$	6	110	7	0.3	0.6	0.007	0.08
37.2	34765	9	48	−0.6	$-\sqrt{3}$	6	110	7	0.2	0.55	0.007	0.09
38.5	35367[a]	9	48	−0.6	$-\sqrt{3}$	6	110	7	0.1	0.5	0.007	0.10

[a] Analytical expression by Spoelstra and Monti [9].

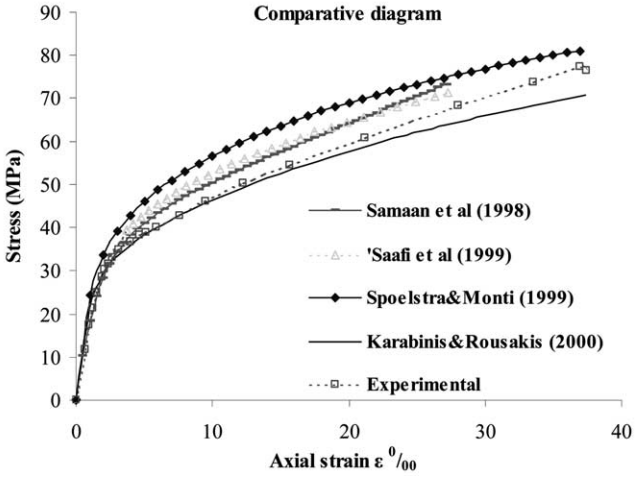

Fig. 10. Comparison of experimental σ–ε values with analytical prediction for specimen of batch C from Mirmiran and Shahawy [2] (10 layers of E-glass FRP tube).

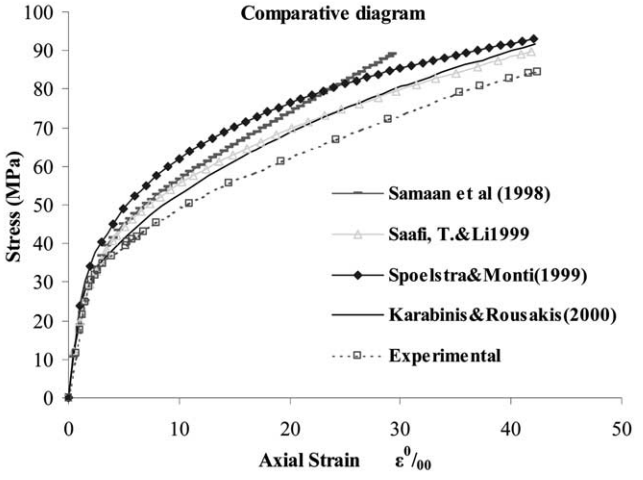

Fig. 11. Comparison of experimental σ–ε values with analytical prediction for specimen of batch C from Mirmiran and Shahawy [2] (14 layers of E-glass FRP tube).

4.2. Fiber-wrapped concrete cylinders

Fiber-wrapped concrete cylinders were tested by Nanni and Bradford [15]. Fifteen cylinders were tested having dimensions 152×305 mm and were wrapped with E-glass fibers and vinylester resin. The hoop strength and modulus of elasticity for the FRP jacket were 583 MPa and 52 000 MPa, respectively. The concrete strength was 36.3 MPa. The comparison of the four models prediction with test results is presented in Fig. 12.

4.3. FRP sheet-confined concrete cylinders

Comparison of the model is made in Fig. 13 against Mastrapa's [18] experimental results for a five-layer

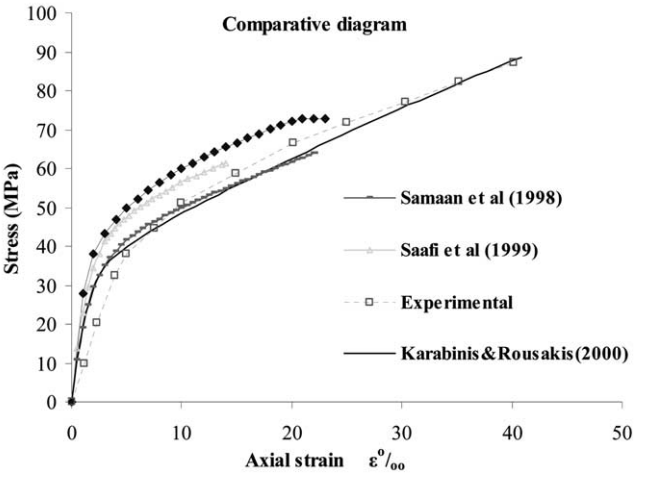

Fig. 12. Comparison of experimental σ–ε values with analytical prediction for specimen from Nanni and Bradford [15] (four layers of E-glass FRP filament).

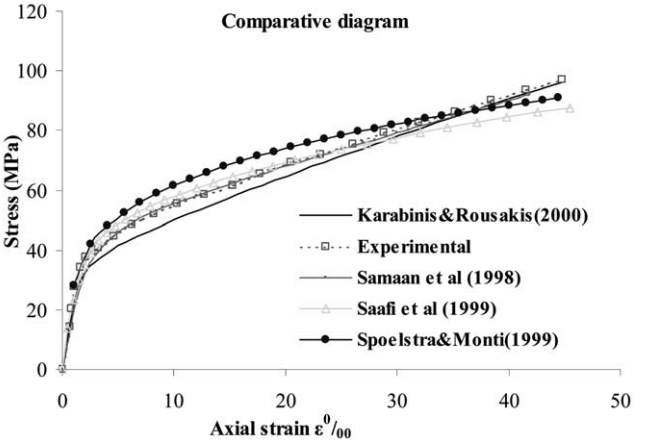

Fig. 13. Comparison of experimental σ–ε values with analytical prediction for specimen of batch 1 from Mastrapa [18] (five layers of S-glass FRP sheet).

S-glass fiber-wrapped concrete cylinder. The specimens were 152.5×305 mm with 37.2 MPa concrete strength and 586 MPa and 20 600 MPa hoop strength and modulus, respectively. In Figs. 14–16 the four models are compared against test results of the present experimental study [16].

From the comparison between the experimental data and the predicted curves, a satisfactory agreement is observed for the proposed model. The proposed model reproduces accurately the general bilinear behavior of the FRP-confined concrete and offers a safer and more accurate prediction.

5. Conclusions

The experimental investigation of the performance of carbon FRP sheet, as a confining means, indicates that

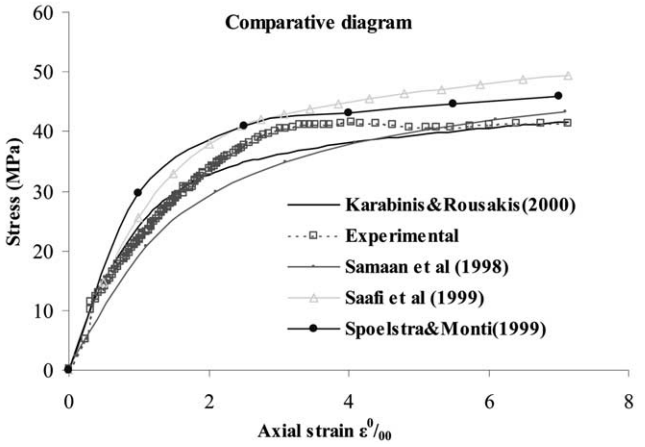

Fig. 14. Comparison of experimental σ–ε values with analytical prediction for specimen C2 from Karabinis and Rousakis [16] (one layer of carbon FRP sheet).

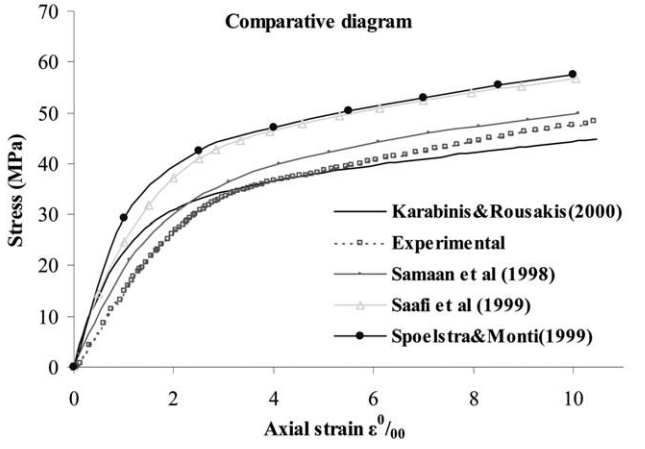

Fig. 15. Comparison of experimental σ–ε values with analytical prediction for specimen C11 from Karabinis and Rousakis [16] (two layers of carbon FRP sheet).

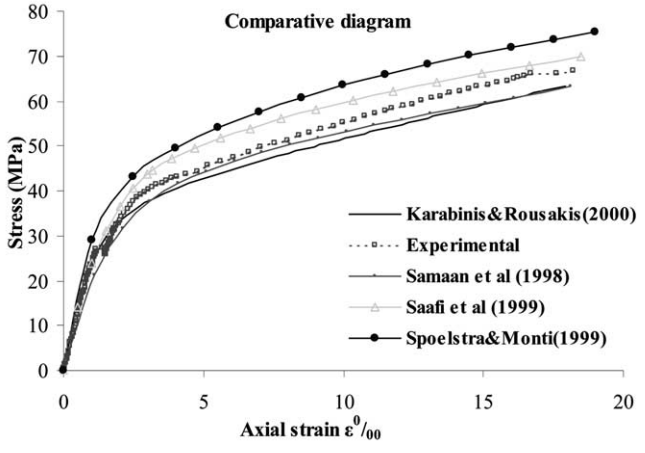

Fig. 16. Comparison of experimental σ–ε values with analytical prediction for specimen C13 from Karabinis and Rousakis [16] (three layers of carbon FRP sheet).

FRP can effectively enhance the strength and ductility of concrete as well as energy absorption, even at low volumetric ratios (ρ_j). The stiffness of the confining mean is the main design parameter. The variation of results indicates the need for the determination of minimum values of the volumetric ratio of reinforcement along with development of FRP application guidelines and quality control for elimination of such problems. A simple model based on non-associative plasticity theory is proposed for the prediction of stress–strain behavior of FRP-confined cylindrical columns. The model takes into account the specific characteristics of the dilatation of confined concrete. The predictions of the model are compared against the experimental data and three existing models. From the comparison it can be concluded that the predicted bilinear behavior of the composite system is accurate enough. Of course, an extension of the calibration to other strengths of concrete (lower and higher) is required to cover structural applications.

References

[1] Saadatmanesh H, Ehsani MR, Li MW. Strength and ductility of concrete columns externally reinforced with fiber composite straps. Struct J ACI 1994;91(4):434–47.
[2] Mirmiran A, Shahawy M. Behavior of concrete columns confined by fiber composites. J Struct Eng ASCE 1997;123(5):583–90.
[3] Samaan M, Mirmiram A, Shahawy M. Model of concrete confined by fiber composites. J. Struct. Eng. ASCE 1998;124(9):1025–31.
[4] Harries KA, Kestner J, Pessiki S, Sause R, Ricles J. Axial behavior of reinforced concrete columns retrofit with FRPC jackets. In: Second International Conference on Composites in Infrastructure, Tucson. 1998. p. 411–25.
[5] Machida A, editor. State-of-the-art report on continuous fiber reinforcing materials. Second Research Committee on CFRM, Japan Society of Civil Engineers: Concrete Engineering Series 3. Tokyo, October 1993.
[6] ACI Committee 440R-96. State-of-the-art report on fiber reinforced plastic reinforcement for concrete structures. American Concrete Institute, Detroit 1996.
[7] Saafi M, Toutanji HA, Li Z. Behavior of concrete columns confined with fiber reinforced polymer tubes. ACI Mater. J. 1999;96(4):500–9.
[8] Harmon TG, Ramakrishnan S, Wang EH. Moment–curvature relationships for confined concrete columns. In: Second International Conference on Composites in Infrastructure, Tucson. 1998. p. 385–97.
[9] Spoelstra MR, Monti G. FRP-confined concrete model. J. Compos. Construct. ASCE 1999;3(3):143–50.
[10] Karabinis AI, Kiousis PD. Plasticity computations for the design of the ductility of circular concrete columns. Comput. Struct. 1996;60(5):825–35.
[11] Scherer J. S&P Sintecno, FRP—Polymer fibers in strengthening. User guide, Brunnen, 1999.
[12] Karabinis ÁI, Kiousis PD. Effects of confinement on concrete columns: plasticity approach. J. Struct. Eng. ASCE 1994;120(9):2747–67.
[13] Karabinis ÁI, Kiousis PD. Strength and ductility of rectangular concrete columns—a plasticity approach. J Struct Eng ASCE 1996;122(3):267–74.

[14] Chen WF. Plasticity in reinforced concrete. McGraw-Hill, 1982.
[15] Nanni A, Bradford NM. FRP jacketed concrete under uniaxial compression. Construct Build Mater 1995;9(2):115–24.
[16] Karabinis AI, Rousakis TC. Cylindrical concrete elements confined by carbon fibers under axial load. 1st Greek Conference of Composite Materials in Concrete, 2000, Xanthi, pp. 287–296.
[17] Karabinis AI, Rousakis TC. Analytical modeling of the mechanical behavior of concrete confined by composite material sheet. 1st Greek Conference of Composite Materials in Concrete, 2000, Xanthi, pp. 308–316.
[18] Mastrapa JC. Effect of construction bond on confinement with fiber composites. MS thesis, University of Central Florida, Orlando, FL, 1997.